Journal of Sound and Vibration (1999) **226**(5), 985–1010
Article No. jsvi.1999.2336, available online at http://www.idealibrary.com on IDEAL®

GEOMETRICAL NON-LINEAR, STEADY STATE, FORCED, PERIODIC VIBRATION OF PLATES, PART II: STABILITY STUDY AND ANALYSIS OF MULTI-MODAL RESPONSE

P. RIBEIRO† AND M. PETYT

Institute of Sound and Vibration Research, University of Southampton, Southampton SO17 1BJ, England

(*Received* 28 *August* 1998, *and in final form* 23 *April* 1999)

The steady state, geometrically non-linear, periodic vibration of rectangular thin plates under harmonic external excitations, is analyzed using the hierarchical finite element and the harmonic balance methods. Modal coupling due to internal resonance is detected and the consequent multi-modal and multi-frequency response is demonstrated. The stability of the obtained solutions is investigated by studying the evolution of perturbations to the solutions and using Floquet's theory.

1. INTRODUCTION

As the displacement amplitude of a fully clamped plate increases, the stiffnes increases due to the effect of the membrane forces. Therefore, the non-linear normal mode [1] is amplitude dependent [2–6] and the resonance frequency changes with the vibration amplitude. Consequently, the natural frequencies may become commensurable that is, a relation of the form $m_1\omega_1 + m_2\omega_2 + \cdots + m_n\omega_n \cong 0$, where m_i are positive or negative integers, may exist.

In non-linear systems, the commensurability of natural frequencies results in coupling of the normal modes and may cause their strong interaction. As a result energy is interchanged between these modes, and multi-frequency, multi-modal response occurs. This phenomenon is known as internal resonance [7, 8].

Modal interactions due to the non-linearity may cause large-amplitude response of modes which linear analysis predicts to remain unexcited. In reference [9], theoretical and experimental studies on the influence of modal interactions on the non-linear response of harmonically excited structural systems are reviewed, and it is concluded that different experiments have shown the existence of internal resonances. In reference [10] experimental evidence of energy transfer between modes in a composite plate was presented.

† Present address: DEMEGI, Faculdade de Engenharia, Universidade do Porto, Rua dos Baragas, 4050-123 Porto, Portugal

0022-460X/99/400985 + 26 $30.00/0

Lau *et al.* [11, 12] used the finite element method and the harmonic balance method (HBM) to study the free and steady state forced vibration of isotropic plates. By using two harmonics, loops of the response curves due to 1 : 3 internal resonances were found. The stability of the solutions was not investigated.

Abe *et al.* [13] analyzed internal resonances in laminated plates. The transverse deflection was assumed to be a function of two linear—therefore constant—modes and the Galerkin's procedure was applied in conjunction with the method of multiple scales. Hence, the method is only valid for displacements smaller than the thickness of the plate. The middle plane in-plane displacement were neglected.

In references [14, 15] the free vibration of isotropic and laminated plates was investigated by the hierarchical finite element method (HFEM) and the harmonic balance method. Internal resonances were detected. They resulted either in a secondary branch of the backbone curve (curve that relates the frequency with the amplitude of vibration) or in an increase in the curvature of a main branch (a main branch originates from a linear solution). Because of coupling between modes vibrating at different frequencies, internal resonances also resulted in a very significant variation of the mode shape during the period of vibration.

To study internal resonances by the HBM more than one harmonic must be introduced in the time series, consequently increasing the number of degrees of freedom of the system. Thus, it would be of great importance to possess an accurate spatial model with a small number of d.o.f. It has been demonstrated, that an accurate model for periodic vibration of plates can be constructed by the hierarchical finite element and the harmonic balance methods, with a reduced number of degrees of freedom in both free [14, 15] and forced vibration [16].

In this paper, the occurrence and the effects of internal resonance on the geometrical non-linear forced vibration of plates are investigated. The model used is based on the HFEM and on the HBM and has been presented in reference [16]. The stability of the obtained solutions is studied and it is demonstrated that stable multi-modal solutions indeed occur. The effect of changing the orientation of the fibers in laminated plates is investigated.

2. STABILITY OF THE SOLUTIONS

An equilibrium solution is said to be locally unstable, if a small perturbation of the solution leads to a departure from it. The converse occurs near a stable equilibrium condition. In a non-linear system more than a single equilibrium solution may appear, but not all the solutions are stable, and it is important to carry out a stability study [7, 8].

To investigate the local stability of the solution a small disturbance is added to the steady state solution

$$\{\tilde{\mathbf{q}}\} = \{\mathbf{q}_w\} + \{\delta\mathbf{q}_w\} \tag{1}$$

and its evolution is studied. If $\{\delta\mathbf{q}_w\}$ dies out with time then $\{\mathbf{q}_w\}$ is stable, if it grows then $\{\mathbf{q}_w\}$ is unstable.

Inserting the disturbed solution (1) into equations of motion (14) of reference [16], expanding the non-linear terms by means of Taylor series around $\{\mathbf{q}_w\}$ and ignoring terms of order higher than $\{\delta\mathbf{q}_w\}$, the following equations are obtained:

$$[\mathbf{M}_b]\{\delta\ddot{\mathbf{q}}_w\} + \frac{\beta}{\omega}[\mathbf{M}_b]\{\delta\dot{\mathbf{q}}_w\} + [\mathbf{K}_{1b}]\{\delta\mathbf{q}_w\} + \frac{\partial([\mathbf{K}nl]\{\mathbf{q}_w\})}{\partial\{\mathbf{q}_w\}}\{\delta\mathbf{q}_w\} = \{\mathbf{0}\}. \quad (2)$$

The coefficients $\partial([\mathbf{K}nl]\{\mathbf{q}_w\})/\partial\{\mathbf{q}_w\}$ depending quadratically on $\{\mathbf{q}_w\}$, are periodic functions of time and can be expanded in a Fourier series:

$$\frac{\partial([\mathbf{K}nl]\{\mathbf{q}_w\})}{\partial\{\mathbf{q}_w\}} = [\mathbf{p}_1] + [\mathbf{p}_2]\cos(2\omega t) + [\mathbf{p}_3]\sin(2\omega t) + [\mathbf{p}_4]\cos(4\omega t) + [\mathbf{p}_5]\sin(4\omega t) + \text{h.o.t.} \quad (3)$$

where h.o.t. stands for higher order terms, which will be neglected. The Fourier coefficients of $\partial([\mathbf{K}nl]\{\mathbf{q}_w\})/\partial\{\mathbf{q}_w\} - [\mathbf{p}_1], [\mathbf{p}_2], [\mathbf{p}_3], [\mathbf{p}_4]$ and $[\mathbf{p}_5]$ – are quadratic functions of $\{\mathbf{q}_w\}$ and can be written in the form

$$[\mathbf{p}_1] = \frac{1}{T}\int_0^T \frac{\partial}{\partial q_w}([\mathbf{K}nl]\{\mathbf{q}_w\})\,\mathrm{d}t, \quad (4)$$

$$[\mathbf{p}_2] = \frac{2}{T}\int_0^T \frac{\partial}{\partial q_w}([\mathbf{K}nl]\{\mathbf{q}_w\})\cos(2\omega t)\,\mathrm{d}t, \quad (5)$$

$$[\mathbf{p}_3] = \frac{2}{T}\int_0^T \frac{\partial}{\partial q_w}([\mathbf{K}nl]\{\mathbf{q}_w\})\sin(2\omega t)\,\mathrm{d}t, \quad (6)$$

$$[\mathbf{p}_4] = \frac{2}{T}\int_0^T \frac{\partial}{\partial q_w}([\mathbf{K}nl]\{\mathbf{q}_w\})\cos(4\omega t)\,\mathrm{d}t, \quad (7)$$

$$[\mathbf{p}_5] = \frac{2}{T}\int_0^T \frac{\partial}{\partial q_w}([\mathbf{K}nl]\{\mathbf{q}_w\})\sin(4\omega t)\,\mathrm{d}t. \quad (8)$$

Inserting equation (3) into the variational equation (2), results in

$$[\mathbf{M}_b]\{\delta\ddot{\mathbf{q}}_w\} + \frac{\beta}{\omega}[\mathbf{M}_b]\{\delta\dot{\mathbf{q}}_w\} + [\mathbf{K}_{1b}]\{\delta\mathbf{q}_w\} + [\mathbf{p}_1] + [\mathbf{p}_2]\cos(2\omega t) + \{\mathbf{p}_3\}\sin(2\omega t) + [\mathbf{p}_4]\cos(4\omega t) + [\mathbf{p}_5]\sin(4\omega t)]\{\delta\mathbf{q}_w\} = \{0\}, \quad (9)$$

which forms a system of Hill's equations [7].

The modal co-ordinates, $\{\delta\boldsymbol{\xi}\}$, of the linear system are defined by

$$\{\delta\mathbf{q}_w\} = [\mathbf{B}]\{\delta\boldsymbol{\xi}\}, \quad (10)$$

where $[\mathbf{B}]$ represents the modal matrix. The modal co-ordinates are normalized so that the matrix of modal masses is the identity matrix.

Using modal co-ordinates, multiplying equation (9) by $[\mathbf{B}]^{\mathrm{T}}$ and introducing a new vector of variables defined as

$$\{\delta\boldsymbol{\xi}\} = \mathrm{e}^{-(1/2)(\beta/\omega)[\mathbf{I}]t}\{\delta\bar{\boldsymbol{\xi}}\}, \tag{11}$$

one obtains the following system equations:

$$\{\delta\ddot{\bar{\boldsymbol{\xi}}}\} + \left([\boldsymbol{\omega}_j^2] - \frac{1}{4}\left(\frac{\beta}{\omega}\right)^2[\mathbf{I}] + [\mathbf{B}]^{\mathrm{T}}([\mathbf{p}_1] + [\mathbf{p}_2]\cos(2\omega t) + [\mathbf{p}_3]\sin(2\omega t) + [\mathbf{p}_4]\cos(4\omega t) + [\mathbf{p}_5]\sin(4\omega t)[\mathbf{B}])\right)\{\delta\bar{\boldsymbol{\xi}}\} = \{\mathbf{0}\}. \tag{12}$$

The simplification to equation (12) was possible only because, after transformation into modal co-ordinates, the damping matrix is equal to a scalar times the identity matrix.

To determine simple instabilities, the solution is assumed to have the form [17]

$$\{\delta\bar{\boldsymbol{\xi}}\} = \mathrm{e}^{\lambda_1}(\{\mathbf{b}_1\}\cos(\omega t) + \{\mathbf{a}_1\}\sin(\omega t) + \{b_3\}\cos(3\omega t) + \{\mathbf{a}_3\}\sin(3\omega t)), \tag{13}$$

where λ are the characteristic exponents. With this expression, simple instabilities of first and of third order will be detected.

Inserting equation (13) into equation (12) and applying the HBM one arrives at the following system of equations:

$$(\lambda^2[\mathbf{I}] + \lambda[\mathbf{M}_1] + [\mathbf{M}_0])\{\mathbf{X}\} = \{\mathbf{0}\}, \tag{14}$$

where $[\mathbf{I}]$ is the identity matrix and $\{\mathbf{X}\}^{\mathrm{T}} = \lfloor\, \mathbf{b}_1 \;\; \mathbf{a}_1 \;\; \mathbf{b}_3 \;\; \mathbf{a}_3 \,\rfloor^{\mathrm{T}}$. The symmetric matrix $[\mathbf{M}_0]$ is defined by [18]

$$[\mathbf{M}_0] = \begin{bmatrix} [\mathbf{B}]^{\mathrm{T}}[\mathbf{p}_1][\mathbf{B}] + \frac{1}{2}[\mathbf{B}]^{\mathrm{T}}[\mathbf{p}_2][\mathbf{B}] + \mathbf{Const}1 & \frac{1}{2}[\mathbf{B}]^{\mathrm{T}}[\mathbf{p}_3][\mathbf{B}] \\ \frac{1}{2}[\mathbf{B}]^{\mathrm{T}}[\mathbf{p}_3][\mathbf{B}] & [\mathbf{B}]^{\mathrm{T}}[\mathbf{p}_1][\mathbf{B}] - \frac{1}{2}[\mathbf{B}]^{\mathrm{T}}[\mathbf{p}_2][\mathbf{B}] + \mathbf{Const}1 \\ \frac{1}{2}[\mathbf{B}]^{\mathrm{T}}[\mathbf{p}_2][\mathbf{B}] + \frac{1}{2}[\mathbf{B}]^{\mathrm{T}}[\mathbf{p}_4][\mathbf{B}] & -\frac{1}{2}[\mathbf{B}]^{\mathrm{T}}[\mathbf{p}_3][\mathbf{B}] + \frac{1}{2}[\mathbf{B}]^{\mathrm{T}}[\mathbf{p}_5][\mathbf{B}] \\ \frac{1}{2}[\mathbf{B}]^{\mathrm{T}}[\mathbf{p}_3][\mathbf{B}] + \frac{1}{2}[\mathbf{B}]^{\mathrm{T}}[\mathbf{p}_5][\mathbf{B}] & \frac{1}{2}[\mathbf{B}]^{\mathrm{T}}[\mathbf{p}_2][\mathbf{B}] - \frac{1}{2}[\mathbf{B}]^{\mathrm{T}}[\mathbf{p}_4][\mathbf{B}] \end{bmatrix}$$

$$\begin{bmatrix} \frac{1}{2}[\mathbf{B}]^{\mathrm{T}}[\mathbf{p}_2][\mathbf{B}] + \frac{1}{2}[\mathbf{B}]^{\mathrm{T}}[\mathbf{p}_4][\mathbf{B}] & \frac{1}{2}[\mathbf{B}]^{\mathrm{T}}[\mathbf{p}_3][\mathbf{B}] + \frac{1}{2}[\mathbf{B}]^{\mathrm{T}}[\mathbf{p}_5][\mathbf{B}] \\ -\frac{1}{2}[\mathbf{B}]^{\mathrm{T}}[\mathbf{p}_3][\mathbf{B}] + \frac{1}{2}[\mathbf{B}]^{\mathrm{T}}[\mathbf{p}_5][\mathbf{B}] & \frac{1}{2}[\mathbf{B}]^{\mathrm{T}}[\mathbf{p}_2][\mathbf{B}] - \frac{1}{2}[\mathbf{B}]^{\mathrm{T}}[\mathbf{p}_4][\mathbf{B}] \\ [\mathbf{B}]^{\mathrm{T}}[\mathbf{p}_1][\mathbf{B}] + \mathbf{Const}2 & 0 \\ 0 & [\mathbf{B}]^{\mathrm{T}}[\mathbf{p}_1][\mathbf{B}] + \mathbf{Const}2 \end{bmatrix}, \tag{15}$$

where the terms **Const**1 and **Const**2 are

$$\mathbf{Const}1 = -\left(\omega^2 + \left(\frac{1}{2}\frac{\beta}{\omega}\right)^2\right)[\mathbf{I}] + [\omega_{0j}^2], \tag{16}$$

$$\mathbf{Const}2 = -\left(9\omega^2 + \left(\frac{1}{2}\frac{\beta}{\omega}\right)^2\right)[\mathbf{I}] + [\omega_{0j}^2], \tag{17}$$

The matrix $[\mathbf{M}_1]$ is

$$[\mathbf{M}_1] = \begin{bmatrix} 0 & 2\omega[\mathbf{I}] & 0 & 0 \\ -2\omega[\mathbf{I}] & 0 & 0 & 0 \\ 0 & 0 & 0 & 6\omega[\mathbf{I}] \\ 0 & 0 & -6\omega[\mathbf{I}] & 0 \end{bmatrix}. \tag{18}$$

Equation (14) is equivalent to the following eigenvalue problem:

$$\begin{bmatrix} 0 & [\mathbf{I}] \\ -[\mathbf{M}_0] & -[\mathbf{M}_1] \end{bmatrix} \begin{Bmatrix} \mathbf{X} \\ \mathbf{\Gamma} \end{Bmatrix} = \lambda \begin{Bmatrix} \mathbf{X} \\ \mathbf{\Gamma} \end{Bmatrix}, \tag{19}$$

where $\{\mathbf{\Gamma}\} = \lambda\{\mathbf{X}\}$.

Because the interest is in the stability of the variable $\{\delta\xi\}$, equation (13) is inserted in equation (11) to obtain

$$\{\delta\xi\} = e^{(\lambda-(1/2)(\beta/\omega))t}(\{\mathbf{b}_1\}\cos(\omega t) + \{\mathbf{a}_1\}\sin(\omega t) + \{\mathbf{b}_3\}\cos(3\omega t) + \{\mathbf{a}_3\}\sin(3\omega t)). \tag{20}$$

If

$$\mathrm{Re}\left(\lambda - \frac{1}{2}\frac{\beta}{\omega}\right) > 0 \tag{21}$$

for any λ, then the solution is unstable, otherwise it is stable. Only the eigenvalue with the major real part must be determined.

The stability study resulted in an eigenvalue problem of the form (19), which is of order $4n$ and, for large n, takes a long computational time to be solved (n is equal to $2p_0^2k$, where k is the number of harmonics used, in this paper $k = 2$). Consequently, simplifications of the stability study are desirable. The sign of the Jacobian's determinant, $|J|$, can be used with this purpose [19, 20].

The Floquet multipliers σ are related to the characteristic or Floquet exponents λ [8] by

$$\lambda = \frac{1}{T}\ln(\sigma), \tag{22}$$

where T is the period of the periodic functions in equation (12). $\{\delta\xi\}$ grows with time when $\|\sigma\|$ crosses the unit circle, which can happen in three ways [21]:

$$\sigma = 1 \Rightarrow \lambda = 0, \tag{23a}$$

$$\sigma = -1 \Rightarrow \lambda \text{ is purely imaginary}, \tag{23b}$$

$$\mathrm{Im}(\sigma) \neq 0 \Rightarrow \lambda \text{ is a complex number}. \tag{23c}$$

For simplicity, in the following paragraph only the mechanism (23a) of losing stability is investigated. In some applications, a pair of complex conjugate characteristic exponents occurred, associated with higher order instabilities. Therefore, higher order instabilities will not be detected by investigating only the mechanism (23a) of losing stability.

From (23a) and due to transformation (11), the stability limit of $\{\delta\boldsymbol{\xi}\}$ is defined by

$$\lambda = \frac{1}{2}\frac{\beta}{\omega}. \tag{24}$$

Inserting expression (24) into (19), one arrives at a condition of the form $|\mathbf{J} + \mathbf{E}| = \mathbf{0}$ [20], where $\mathbf{E}$ is an error matrix. In the numerical applications carried out, this error matrix was not important, and was neglected. Therefore, a study of the first order's stability of the two harmonics solution, using the sign of the determinant of Jacobian matrix as an indicator of a change if stability status, can be carried out. The process is similar to the one suggested in reference [19] for harmonic solutions. However, one should bear in mind that when the model includes the in-plane displacements, the Jacobian used in this work is an approximated one [16].

3. APPLICATIONS

3.1. INTRODUCTION

Two plates are studied, one is isotropic (aluminium DTDSO 70)—Plate 1—and the other is a composite laminated plate (graphite/epoxy)—Plate 2, with five layers. The layers of Plate 2 have the following orientation of principal axes (θ, $-\theta$, θ, $-\theta$, θ). Two values will be assumed for θ: 15° and 45°. The dimensions and the material properties of Plates 1 and 2 are given in reference [16].

In reference [16], the HFEM and HBM model, as well as the continuation method used to solve the equations of motion are presented. Convergence studies were carried out and it was demonstrated that an accurate model of Plate 1 and of 2 with $\theta = 45°$, would include two harmonics, five out-of-plane shape functions and eight in-plane shape functions. In this paper, two harmonics, five out-of-plane and ten in-plane shape functions are utilized to derive the models of both Plate 1 (except when indicated otherwise) and 2, with $\theta = 45°$. Convergence studies for steady state forced vibration of Plate 2 with $\theta = 15°$ will not be carried out, but, based on the free vibration analysis of this same plate [15], a model with two harmonics, six out-of-plane and ten in-plane shape functions will be used ($p_0 = 6$, $p_i = 10$).

3.2. PLATE 1

A harmonic excitation at normal incidence with the form shown in Figure 1 was applied. The expression that gives the amplitude of this force is: $P = 2 + 5 \times 10^4$

$f_2(\xi)f_2(\eta)\,\mathrm{N/m^2}$, where f_2 is the second out-of-plane shape function given by

$$f_2 = (1/8)\,\xi - (1/4)\,\xi^3 + (1/8)\,\xi^5. \tag{25}$$

This excitation has a form very similar to that of the fourth mode of vibration of the plate. The modes of vibration of Plate 1 are presented in reference [14].

Figure 2–4 show the FRF curves of the first and third harmonics calculated at $(\xi, \eta) = (0, 0)$ and of the first harmonic calculated at $(\xi, \eta) = (0{\cdot}5, 0{\cdot}5)$. They have just one peak, which is due to the first mode (mode (1, 1)—the mode numbers (n_1, n_2) are related to the modal lines: n_1 and n_2 are one plus the number of nodal lines crossing any line parallel to the x- and y-axis, respectively. The plate edges are not counted). Figure 5 shows the FRF curve of the third harmonic at $(\xi, \eta) = (0{\cdot}5, 0{\cdot}5)$. There is a very prominent peak, which is due to excitation of mode 4 (or mode (2, 2)). In fact, the relation between the linear natural frequencies of the fourth and first mode is $\omega_{l4}/\omega_{l1} = 3{\cdot}006$, and the fourth mode is excited by means of a 1 : 3 internal resonance. After this peak, the influence of the fourth mode and the amplitude of vibration decreases, and at $W_3/h \cong 0{\cdot}002$, the FRF curve describes almost a semi-circle. Each picture in Figure 6 represents the deformations of the plate—divided by the plate's thickness—associated with each term of the time series. These deformations are calculated by the following expressions:

$$W_{c1} = \lfloor\, \mathbf{N}_w \,\rfloor\{\mathbf{w}_{c1}\}, \tag{26}$$

$$W_{s1} = \lfloor\, \mathbf{N}_w \,\rfloor\{\mathbf{w}_{s1}\}, \tag{27}$$

$$W_{c3} = \lfloor\, \mathbf{N}_w \,\rfloor\{\mathbf{w}_{c3}\}, \tag{28}$$

$$W_{s3} = \lfloor\, \mathbf{N}_w \,\rfloor\{\mathbf{w}_{s3}\}, \tag{29}$$

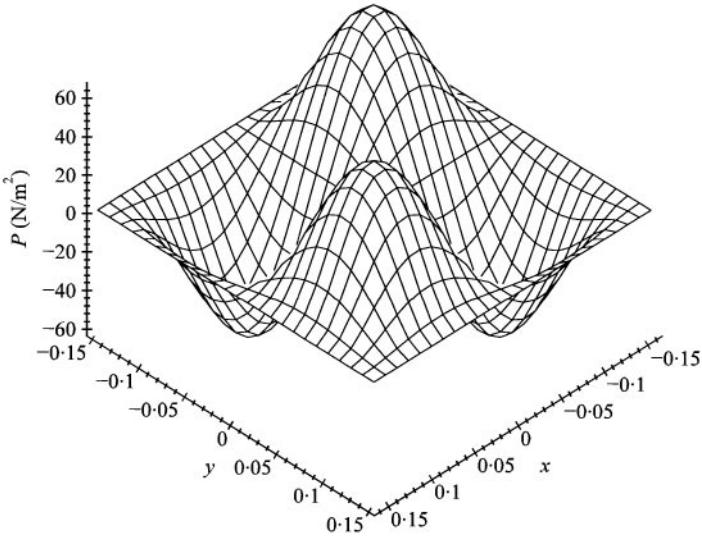

Figure 1. Non-symmetric excitation.

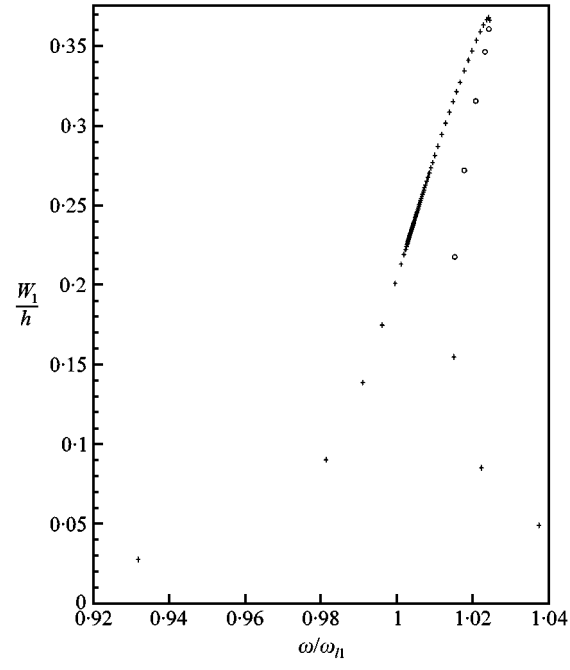

Figure 2. FRF of first harmonic at $(\xi, \eta) = (0, 0)$ due to non-symmetric excitation: + stable; ○ unstable. Plate 1.

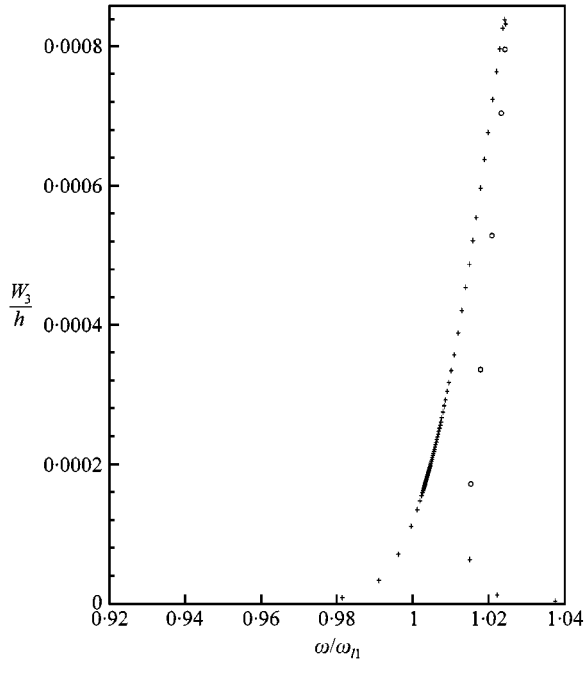

Figure 3. FRF of third harmonic at $(\xi, \eta) = (0, 0)$ due to non-symmetric excitation: + stable; ○ unstable. Plate 1.

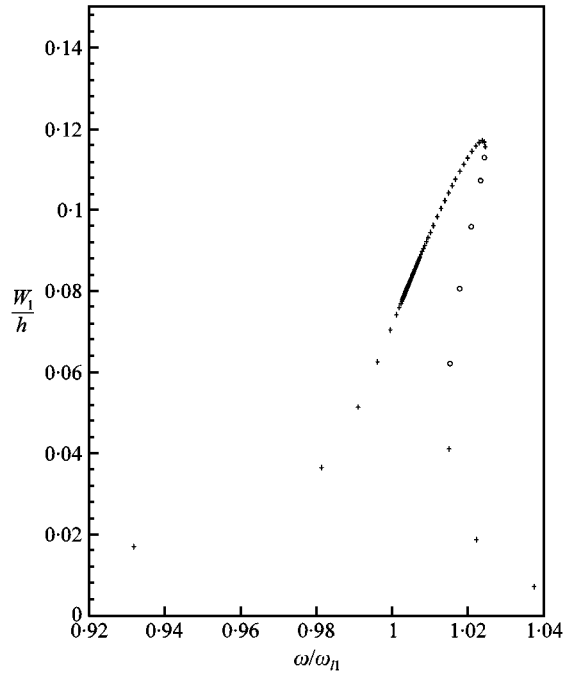

Figure 4. FRF of first harmonic at $(\xi, \eta) = (0{\cdot}5, 0{\cdot}5)$ due to non-symmetric excitation: + stable; ○ unstable. Plate 1.

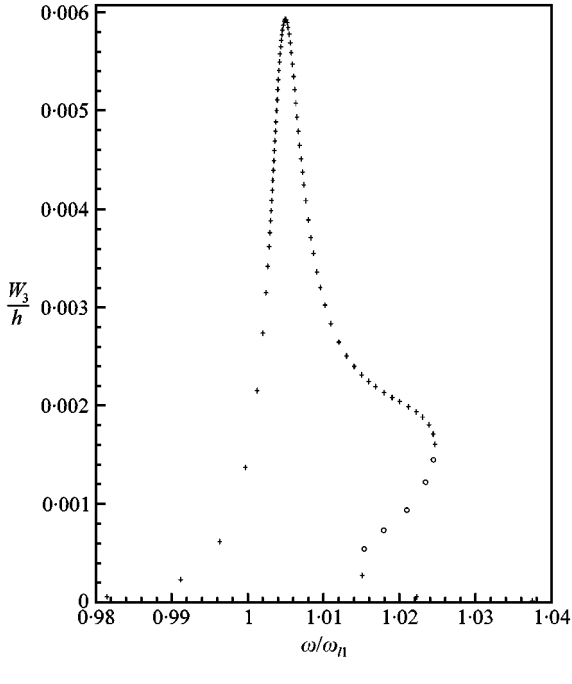

Figure 5. FRF of third harmonic at $(\xi, \eta) = (0{\cdot}5, 0{\cdot}5)$ due to non-symmetric excitation: + stable; ○ unstable. Plate 1.

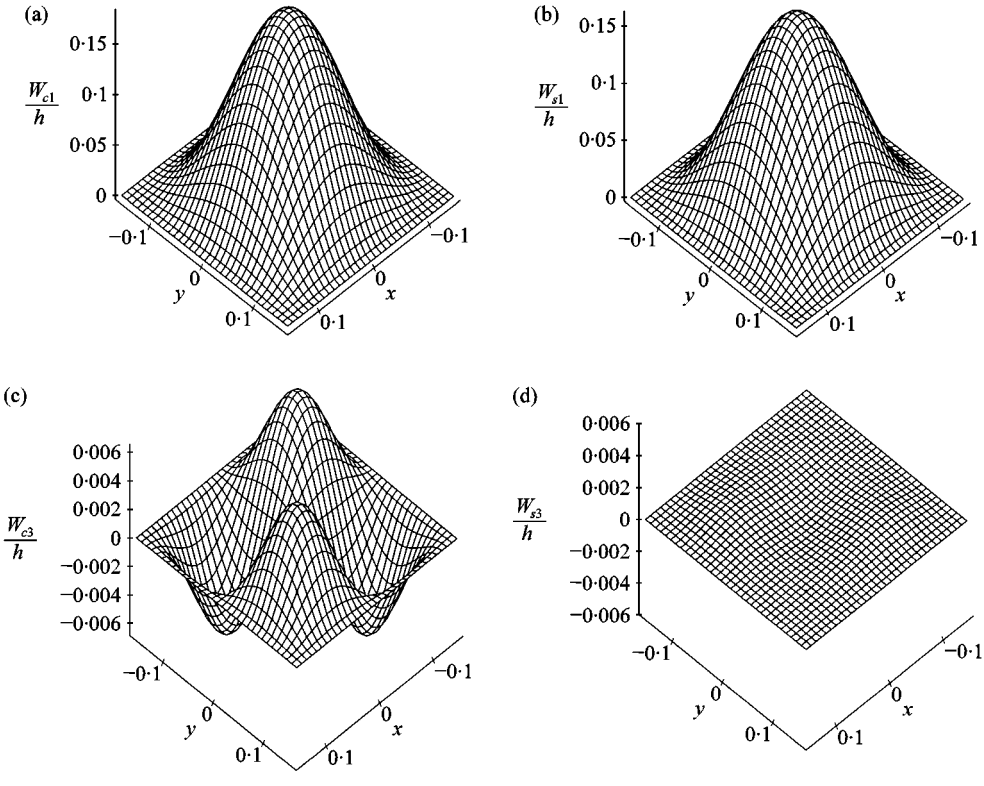

Figure 6. Deformation of Plate 1 at point $\omega/\omega_{l1} = 1{\cdot}0050$. (a) cos ($\omega t$); (b) sin ($\omega t$); (c) cos ($3\omega t$); (d) sin ($3\omega t$).

It is visible that modes one and four define the vibration of the plate. Note that, although the internal resonance occurs at low amplitudes—around $W_1/h = 0{\cdot}25$ at $\{\xi, \eta\} = (0, 0)$ (area of greater point density in Figure 2), it would be disregarded by a harmonic solution.

A normal incident harmonic excitation of large amplitude, 10 N/m^2, was also applied to Plate 1. At large amplitudes it was difficult to achieve convergence when the middle plane in-plane displacements were included in the model, because of the approximated Jacobian used to solve the equations of motion. In order to facilitate convergence, the middle plane in-plane displacements were neglected. The model is therefore not so accurate, but the qualitative study on the effects of modal coupling remains valid. Five out-of-plane shape functions were used.

The first harmonic attained a maximum vibration amplitude of around 1·2 times the thickness of the plate—Figure 7—and the third harmonic 0·23—Figure 8. The shape of the FRF curve at large amplitudes of vibration is different from the typical shape of harmonic solutions, because of the internal resonance. In fact, Figure 9 shows that, at large amplitudes, the vibration of the plate is defined by two non-linear modes: the first—(1, 1)-mode, linked with the first harmonic, and the fifth—(1, 3)—mode, linked with the third harmonic. The linear natural frequencies

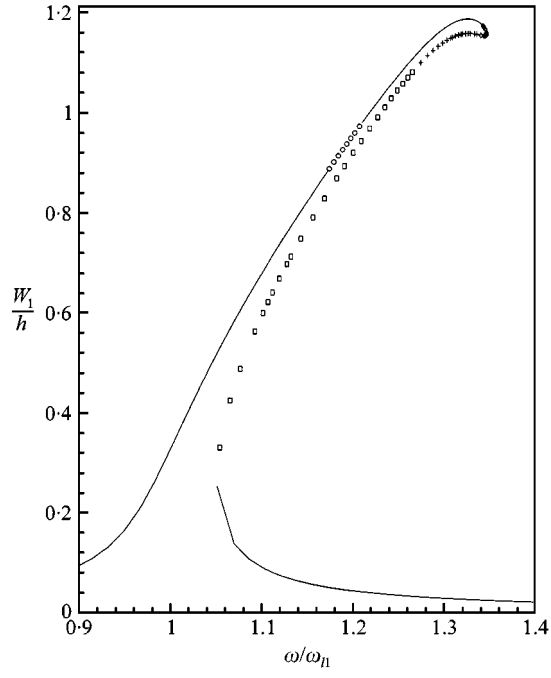

Figure 7. FRF of first harmonic at $(\xi, \eta) = (0, 0)$: − and + stable; ○ and ◇ third order instabilities; □ first order instability. Plate 1.

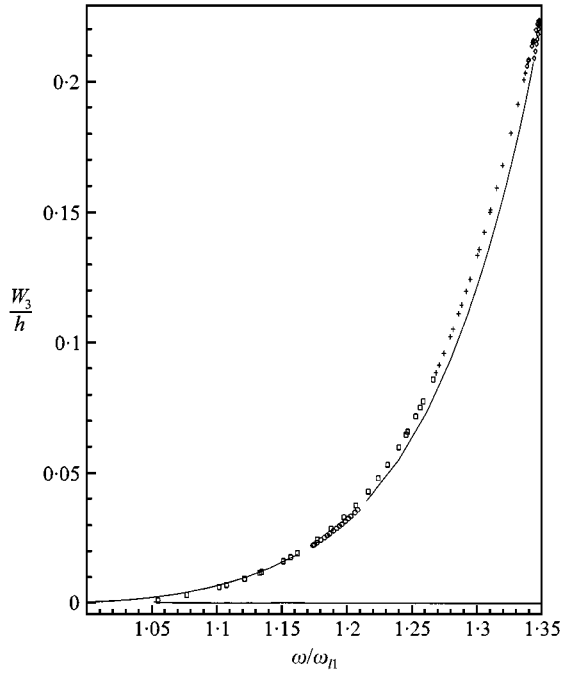

Figure 8. FRF of third harmonic at $(\xi, \eta) = (0, 0)$: − and + stable; ○ and ◇ third order instabilities; □ first order instability.

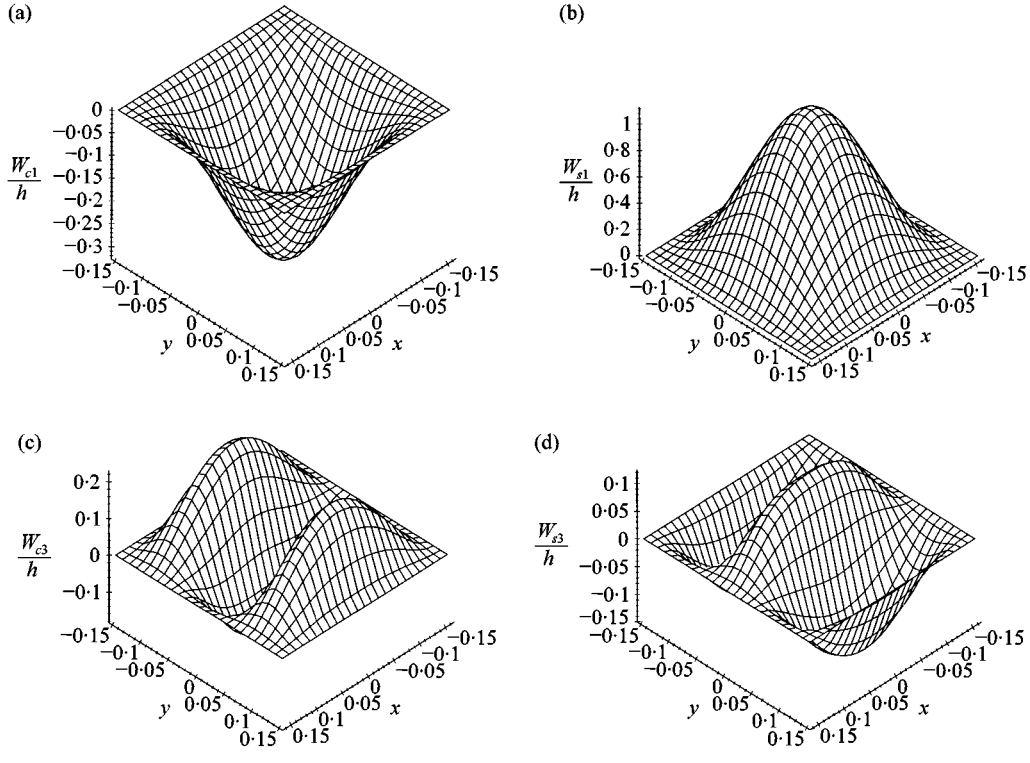

Figure 9. Deformation of Plate 1 at point $\omega/\omega_{l1} = 1{\cdot}34$. (a) cos ($\omega t$); (b) sin ($\omega t$); (c) cos ($3\omega t$); (d) sin ($3\omega t$).

of these modes are related by $\omega_{ls}/\omega_{11} = 3{\cdot}4712$. Due to the geometrical non-linearity, the first resonance frequency increases with the vibration amplitude, the fifth and the first resonance frequencies become related by $\omega_{nl5}/\omega_{nl1} \cong 3$, and there is modal coupling between the first and fifth modes, due to a 1 : 3 internal resonance.

Figures 10–13 show projections of the plate in the plane defined by $x = 0$ at several instants during a period of vibration, T. The amplitude of vibration displacement was divided by the thickness of the plate. The great importance of the third harmonic in the definition of the deformation of the plate is obvious.

The stability of the solutions was studied by solving the eigenvalue problem (19). Three separated instability area were detected by calculating the characteristic exponents: Figure 7. The unstable solutions denoted by a circle are of the third order type: they occur in the vicinity of $\omega_{l5}/3$. In this area the stability was lost by process (23c), that is, a pair of complex conjugate Floquet multipliers crossed the unit cycle. The instability of the solutions denoted by a diamond is probably also of the third order type, as these solutions occur close to $\omega_{l6}/3$. The solutions denoted by a square are unstable, with an instability of the first order, associated with the first resonance frequency. In this last case, the stability was lost with purely real characteristic eigenvalues. Note that several solutions where modal coupling is present are stable.

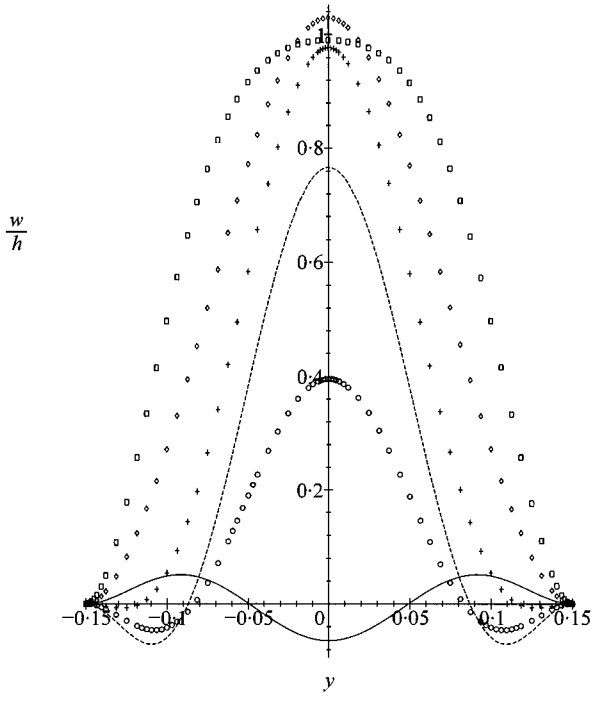

Figure 10. Section of Plate 1 at $x = 0$, frequency $\omega/\omega_{l1} = 1{\cdot}34$: — $t = 0$; ○ $t = (1/24)T$; --- $t = (2/24)T$; + $t = (3/24)T$; ◇ $t = (4/24)T$; □ $t = (5/24)T$.

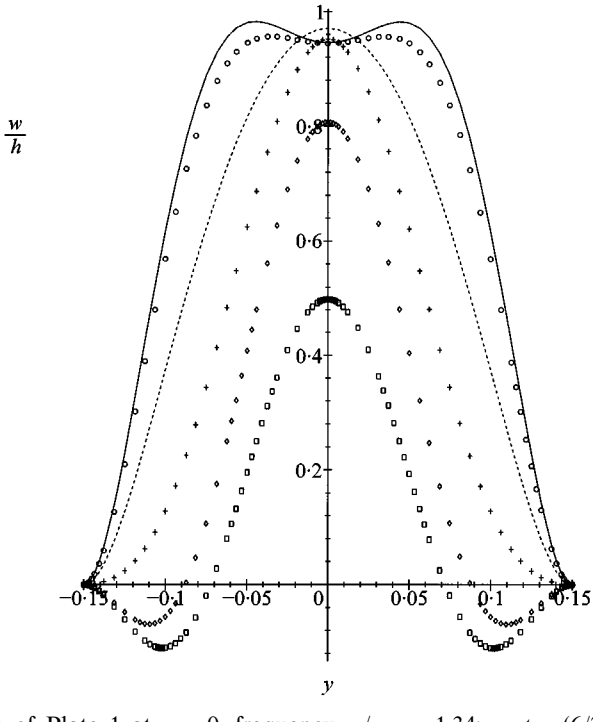

Figure 11. Section of Plate 1 at $x = 0$, frequency $\omega/\omega_{l1} = 1{\cdot}34$: — $t = (6/24)T$; ○ $t = (7/24)T$; --- $t = (8/24)T$; + $t = (9/24)T$; ◇ $t = (10/24)T$; □ $t = (11/24)T$.

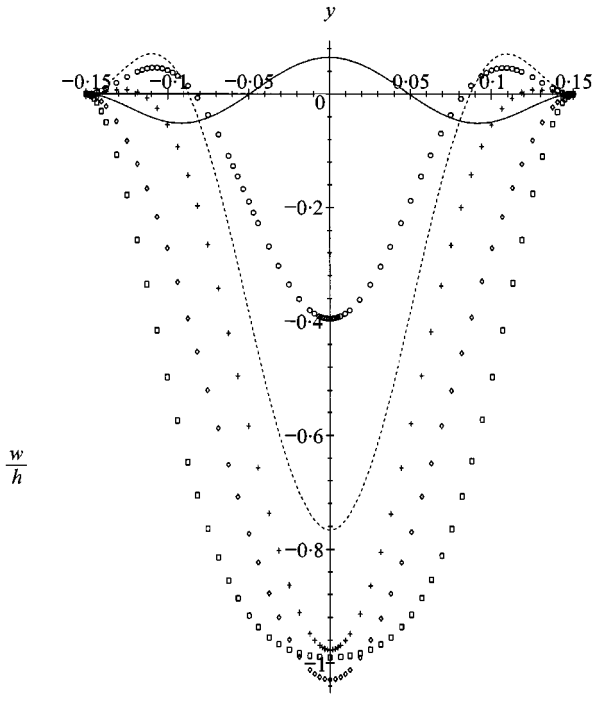

Figure 12. Section of Plate 1 at $x = 0$, frequency $\omega/\omega_{l1} = 1{\cdot}34$: $-$ $t = (12/24)T$; ○ $t = (13/24)T$; --- $t = (14/12)T$; + $t = (15/24)T$; ◇ $t = (16/24)T$; □ $t = (17/24)T$.

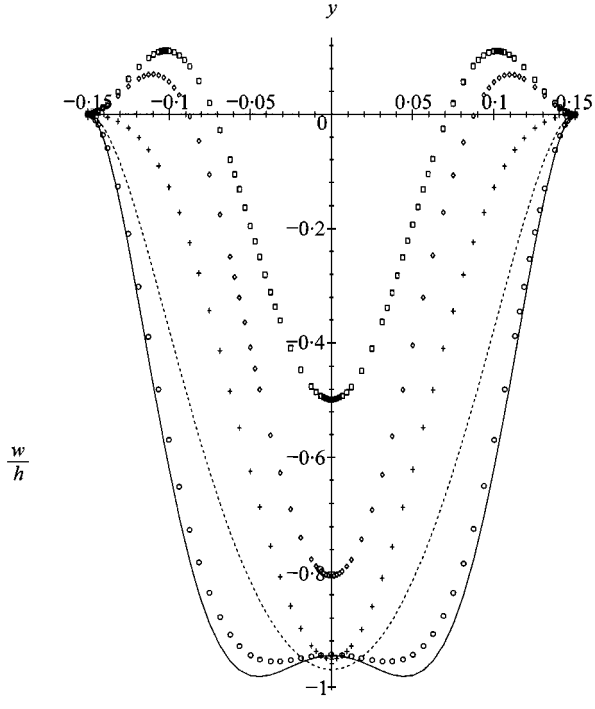

Figure 13. Section of Plate 1 at $x = 0$, frequency $\omega/\omega_{l1} = 1{\cdot}34$: $-$ $t = (18/24)T$; ○ $t = (19/24)T$; --- $t = (20/24)T$; + $t = (21/24)T$; ◇ $t = (22/24)T$; □ $t = (23/24)T$.

A stability study in which only the first order instability was investigated—using the sign of $|\mathbf{J}|$—seems to confirm the previous analysis: only the points represented by a square in Figure 7 were detected as unstable. The Jacobian's determinant, $|\mathbf{J}|$, did not change sign between stable and higher order unstable regions. Because of the approximations followed, more research should be conducted in order to confirm the use of $|\mathbf{J}|$ as an indicator of loss of stability of the first type, when the solution is multi-harmonic.

Super-harmonic resonance of mode 1 was detected, when the excitation frequency is close to $\omega_{l1}/3$. The amplitudes of vibration displacement were extremely low at this resonance.

3.3. PLATE 2

In Figures 20 and 21 of Part I of this paper, which represent the amplitude of the third harmonic of Plate 2, (when not stated otherwise, the orientation of Plate 2's fibers is given by $\theta = 45^\circ$), two peaks are visible. The first one, at $\omega/\omega_{l1} = 0{\cdot}9738$, is due to the excitation of mode number 4. The excitation of this mode was not accounted for by the one harmonic approximation and that is the reason why it gave such poor result (Figure 7 of reference [16]). The second peak of the third harmonic has a round shape, which is due to an additional excitation, namely of mode six, and to a coupling between mode 1 and 6. The natural modes of Plate 2 are presented in reference [15], here it can be seen that the linear natural frequencies of modes one, four and six are related by $\omega_{l4}/\omega_{l1} = 2{\cdot}9081$ and $\omega_{l6}/\omega_{l1} = 3{\cdot}7546$. Due to the variation of the resonance frequencies with the vibration amplitude, 1 : 3 internal resonances occur between these modes.

To make the effect of internal resonance more evident. Plate 2 was excited with a harmonic plane wave also at normal incidence, but with a large amplitude: 5 N/m^2. The frequency response function curves obtained are represented in Figures 14–17. Figures 18–20 represent the non-linear modes involved in the vibration of the plate at three different frequencies, in the following order: $\omega/\omega_{l1} = 0{\cdot}97175$, the first peak of the third harmonic; $\omega/\omega_{l1} = 1{\cdot}0882$, the maximum amplitude of vibration of the third harmonic at $(\xi, \eta) = (0, 0)$; and $\omega/\omega_{l1} = 1{\cdot}1382$, the maximum amplitude of vibration of the third harmonic at $(\xi, \eta) = (0{\cdot}5, 0{\cdot}5)$, and of the first harmonic at both $(\xi, \eta) = (0{\cdot}0)$ and $(\xi, \eta) = (0{\cdot}5, 0{\cdot}5)$.

There are two 1 : 3 successive internal resonances and respective modal couplings due to geometrical non-linearity. The first internal resonance occurs between the first mode and the fourth, and results in the excitation of the fourth mode and in the first peak of both Figures 15 and 17. In fact, the modes associated with the first and third harmonics in Figure 18 are, respectively, the first and the fourth.

The second internal resonance, occurs between the first mode and the sixth.[‡] The increasing importance of modes four and six—which define the vibration of the third harmonic—in the definition of the vibration of the plate is responsible for the

[‡] One can argue that there exists also a 1 : 1 internal resonance between the fourth and the sixth modes of vibration.

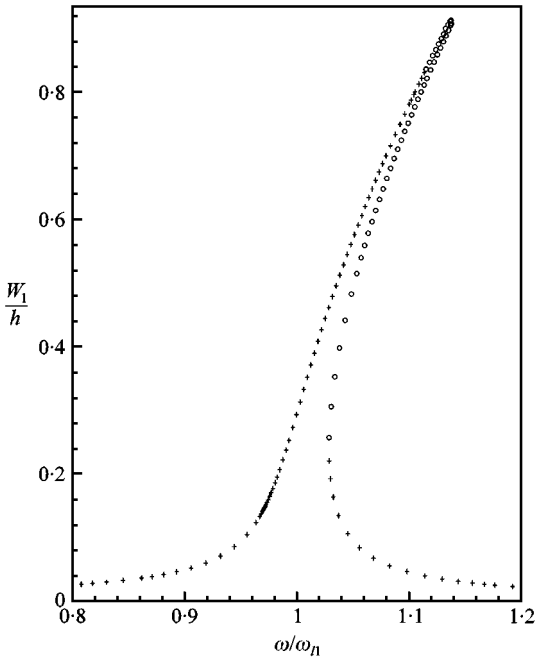

Figure 14. FRF of the first harmonic at $(\xi, \eta) = (0, 0)$: + stable; ○ unstable. Plate 2.

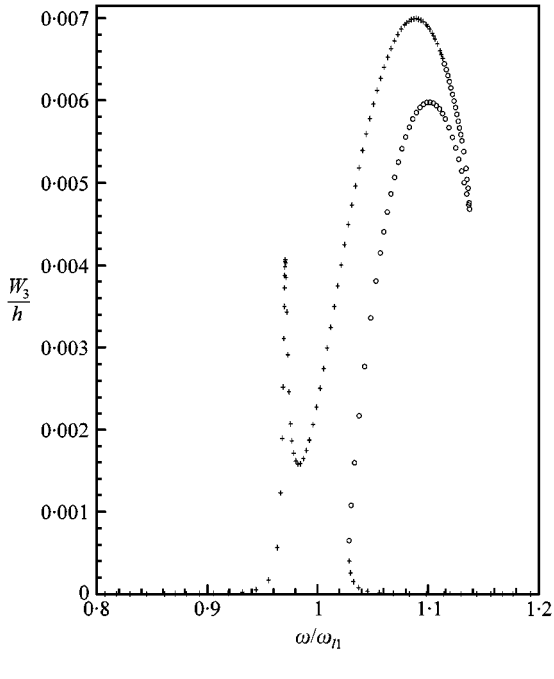

Figure 15. FRF of the third harmonic at $(\xi, \eta) = (0, 0)$: + stable; ○ unstable. Plate 2.

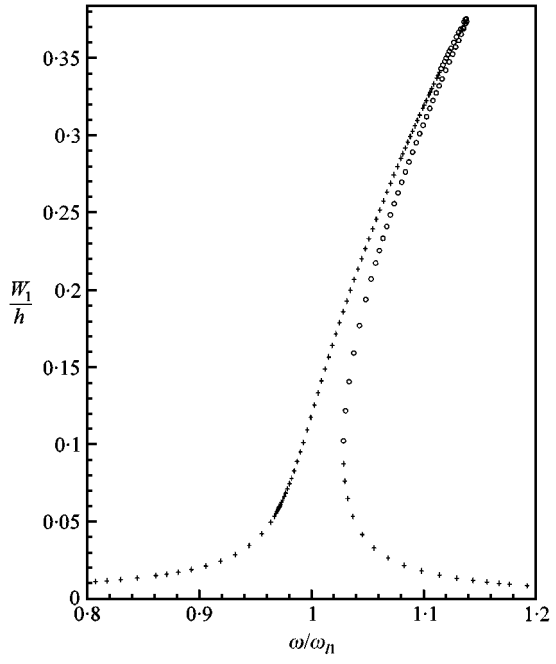

Figure 16. FRF of the first harmonic at $(\xi, \eta) = (0{\cdot}5, 0{\cdot}5)$: + stable; ○ unstable. Plate 2.

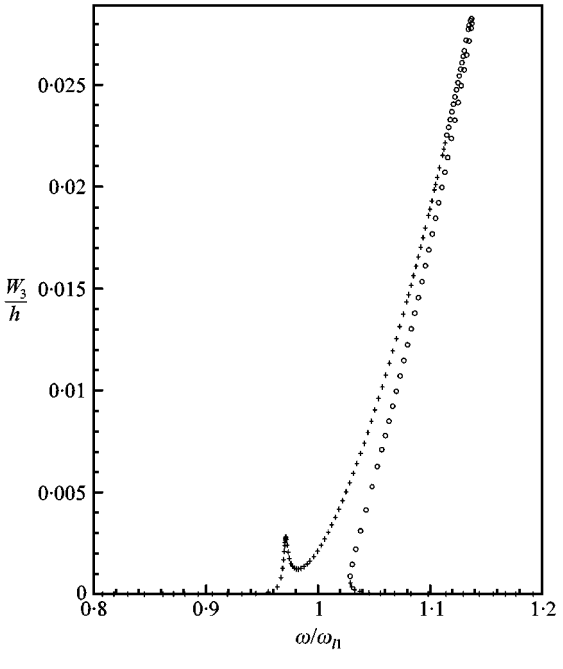

Figure 17. FRF of the third harmonic at $(\xi, \eta) = (0{\cdot}5, 0{\cdot}5)$: + stable; ○ unstable. Plate 2.

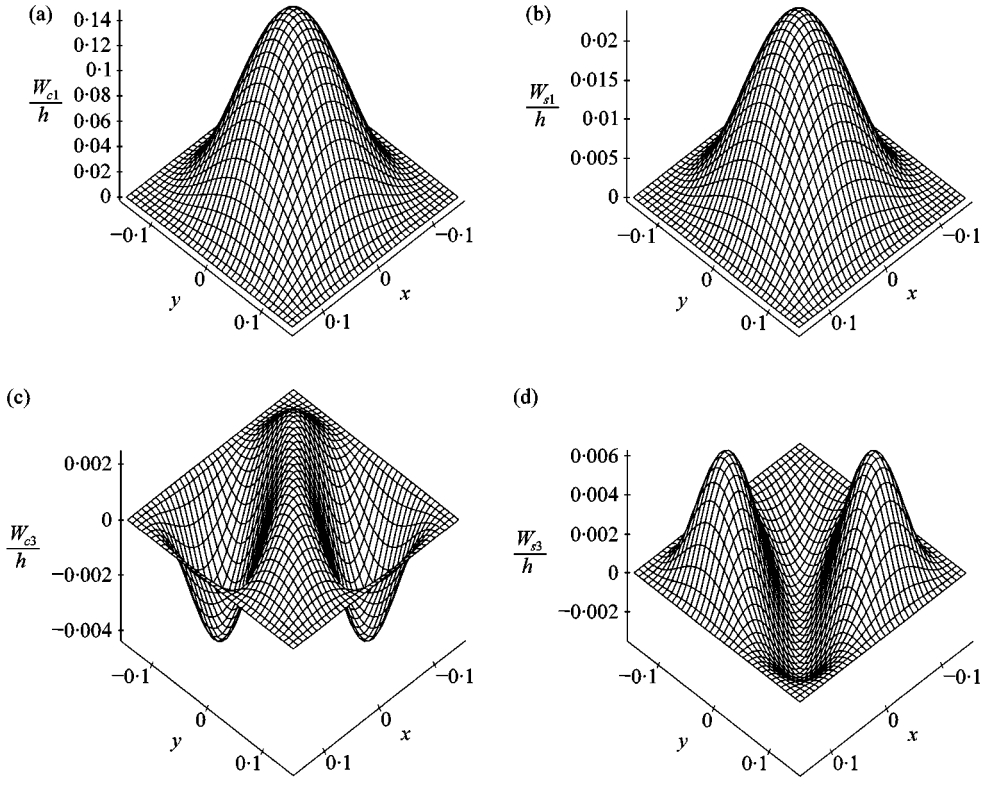

Figure 18. Deformation of Plate 2 at point $\omega/\omega_{l1} = 0{\cdot}97175$. (a) cos ($\omega t$); (b) sin ($\omega t$); (c) cos ($3\omega t$); (d) sin ($3\omega t$).

softening spring effect in the third harmonic, which is visible in Figure 15. In fact, by combining the fourth and sixth linear modes, Figure 21 was created. The similarities between Figure 21 and Figures 19(d) and 20(c), and between Figure 21 and the symmetric with relation to the x–y plane of Figures 19(c) and 20(d) are evident. The modal coupling does not die away with increasing frequencies, therefore, the vibration of the plate at frequencies slightly larger than the first linear resonance frequency involves the first, fourth and sixth modes. The fifth mode of vibration is not visibly excited.

The instabilities which occur in the upper part of the first harmonic's FRF curve in Figures 14 and 16, before the largest amplitude of vibration is achieved, are of the third order type: they occur around $\omega_{l6}/3$.

Figures 22 and 23 display the response of Plate 2 to a harmonic plane wave of 4 N/m^2 of amplitude, at normal incidence, for a wide range of frequencies. These curves were easily and automatically constructed by the continuation method. Only modes which are symmetric with relation to the planes x_1–z and y_1–z, where x_1 and y_1 are axes obtained by rotating the x- and y-axis 45° around the z-axis, are excited and the larger peaks occur near the resonance frequencies of the linear modes. Super-harmonic resonances occur when the frequencies of excitation are

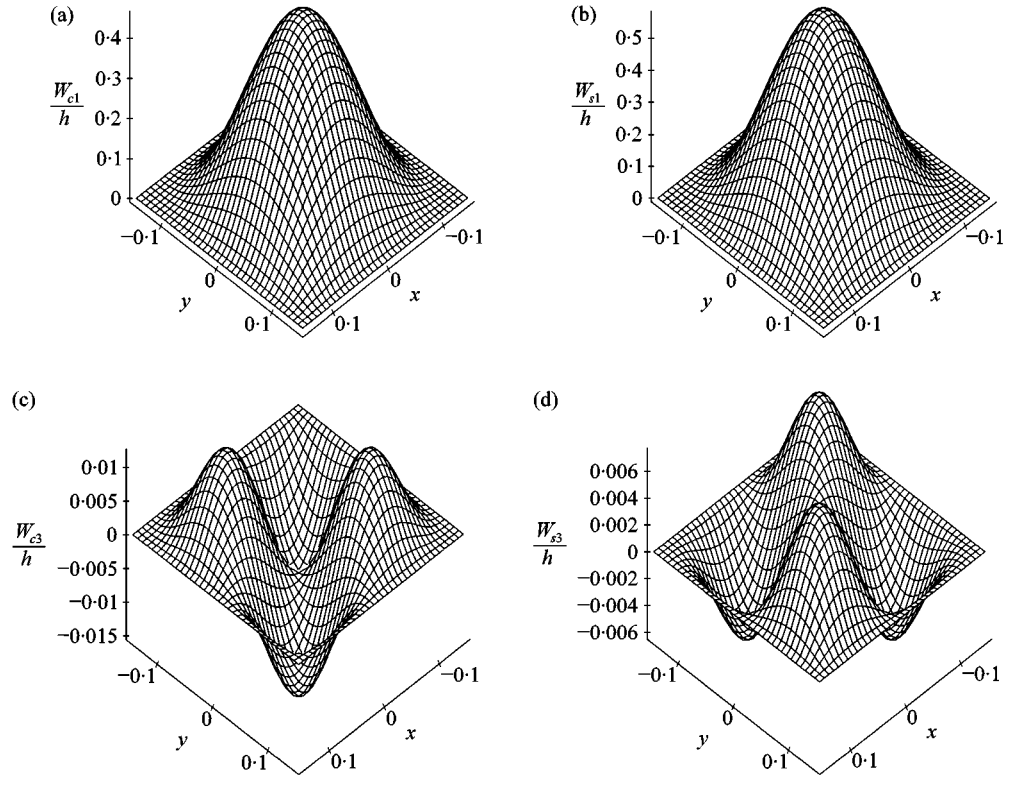

Figure 19. Deformation of Plate 2 at point $\omega/\omega_{l1} = 1{\cdot}0882$. (a) cos ($\omega t$); (b) sin ($\omega t$); (c) cos ($3\omega t$); (d) sin ($3\omega t$).

close to $\omega_{lk}/3$. Their vibration amplitudes are so small, that they are not visible in the figures.

In Figures 24–27, the FRF curves of Plate 2 with $\theta = 45^\circ$ and 15° are compared. The excitation is an harmonic plane wave at normal incidence with 5 N/m^2 of amplitude and the loss factor is $\alpha = 0{\cdot}01$ (which gives a damping factor slightly larger when $\theta = 45^\circ$ than when $\theta = 15^\circ$, because $\omega_{l1} = 763{\cdot}10$ rad/s in the first case and $\omega_{l1} = 799{\cdot}65$ rad/s in the second case).

The slope of the curves is different, showing that the stiffness of Plate 2 increases more with amplitude if $\theta = 15^\circ$ than if $\theta = 45^\circ$. Therefore, for the same excitation amplitude, larger total amplitudes of vibration are attained if $\theta = 45^\circ$. However, due to the internal resonance already reported for Plate 2, $\theta = 45^\circ$, the amplitude of the third harmonic at $(\xi, \eta) = (0, 0)$ is, after frequency $\omega/\omega_{l1} \cong 1{\cdot}11$, greater if $\theta = 15^\circ$ than if $\theta = 45^\circ$.

In Figure 28, the shapes of Plate 2, $\theta = 15^\circ$, associated with each of the terms of the time series, at frequency $\omega/\omega_{l1} \cong 0{\cdot}9666$, first peak of the third harmonic at $(\xi, \eta) = (0{\cdot}5, 0{\cdot}5)$, are shown. This small peak is due to the excitation of the sixth mode.

In Figure 29 the shapes of Plate 2, $\theta = 15^\circ$, connected with each term of the time series, at frequency $\omega/\omega_{l1} \cong 1{\cdot}1331$, higher peak of all harmonics, are shown. The

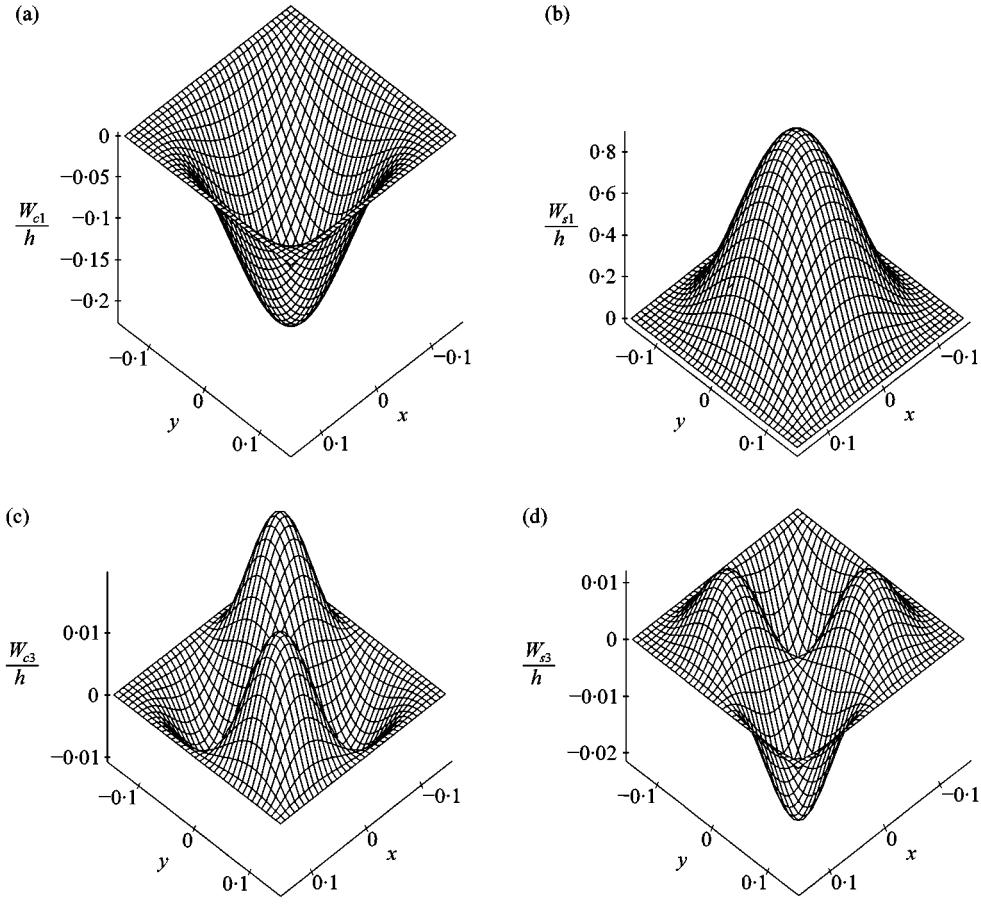

Figure 20. Deformation of Plate 2 at point $\omega/\omega_{l1} = 1{\cdot}1382$. (a) cos ($\omega t$); (b) sin ($\omega t$); (c) cos ($3\omega t$); (d) sin ($3\omega t$).

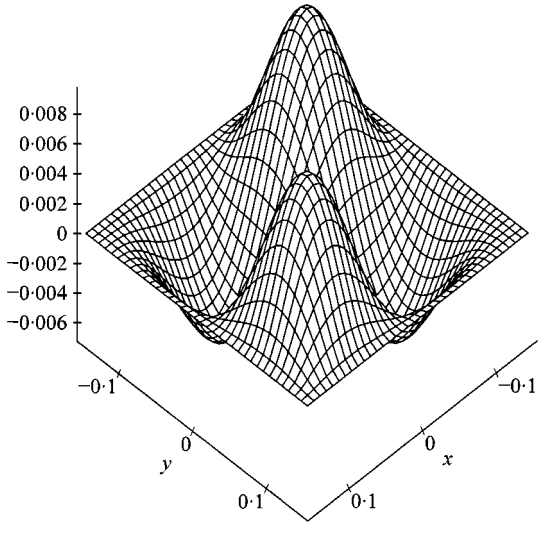

Figure 21. Combination of modes 4 and 6 of Plate 2 ($\theta = 45°$).

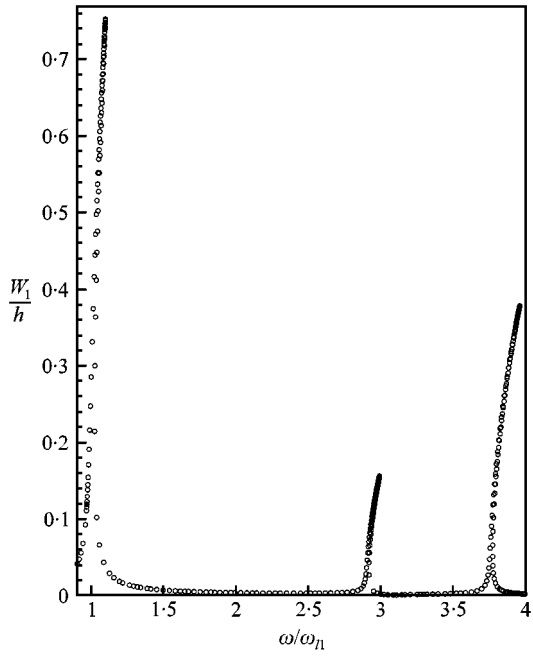

Figure 22. First harmonic FRF at $(\xi, \eta) = (0, 0)$. Plate 2 ($\theta = 45°$).

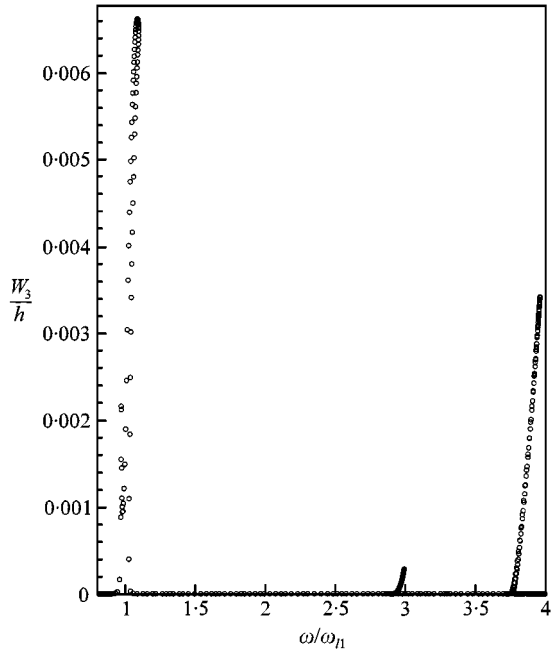

Figure 23. Third harmonic FRF at $(\xi, \eta) = (0, 0)$. Plate 2 ($\theta = 45°$).

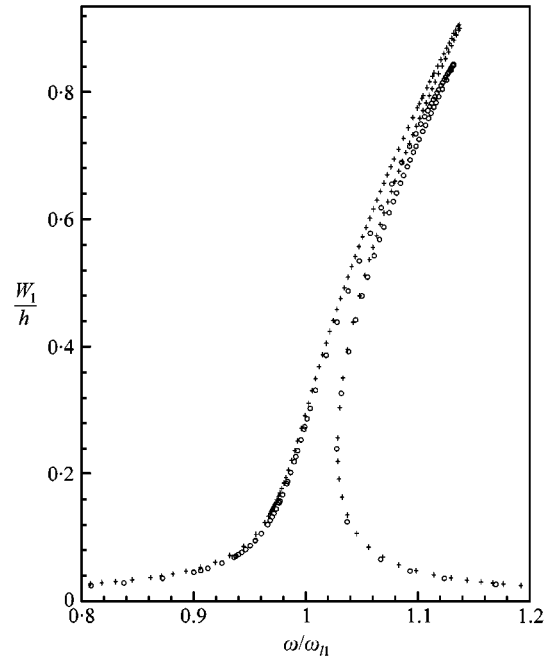

Figure 24. First harmonic FRF at $(\xi, \eta) = (0, 0)$. Plate 2: ○ $\theta = 15°$; + $\theta = 45°$.

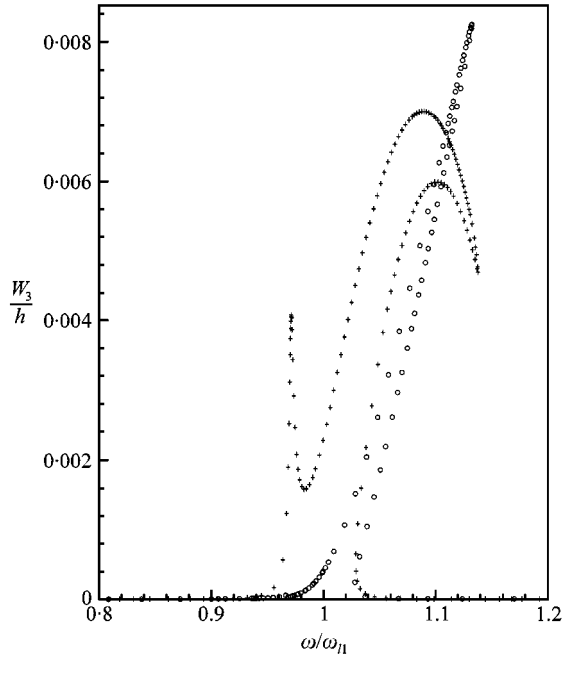

Figure 25. Third harmonic FRF at $(\xi, \eta) = (0, 0)$. Plate 2: ○ $\theta = 15°$; + $\theta = 45°$.

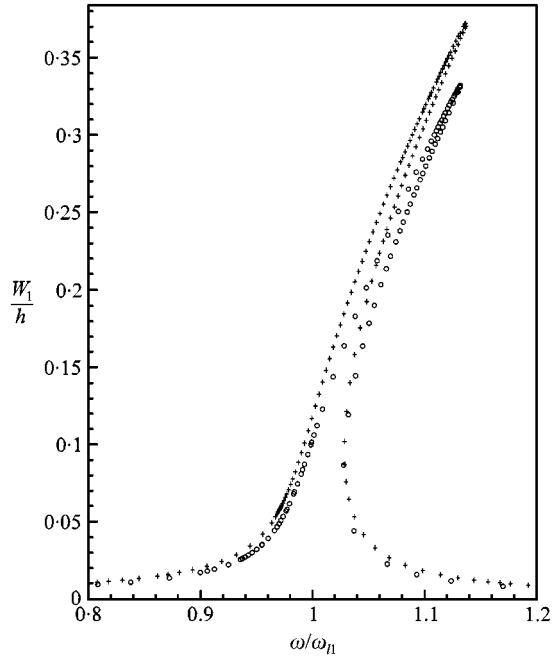

Figure 26. First harmonic FRF at $(\xi, \eta) = (0{\cdot}5, 0{\cdot}5)$. Plate 2: ○ $\theta = 15°$; + $\theta = 45°$.

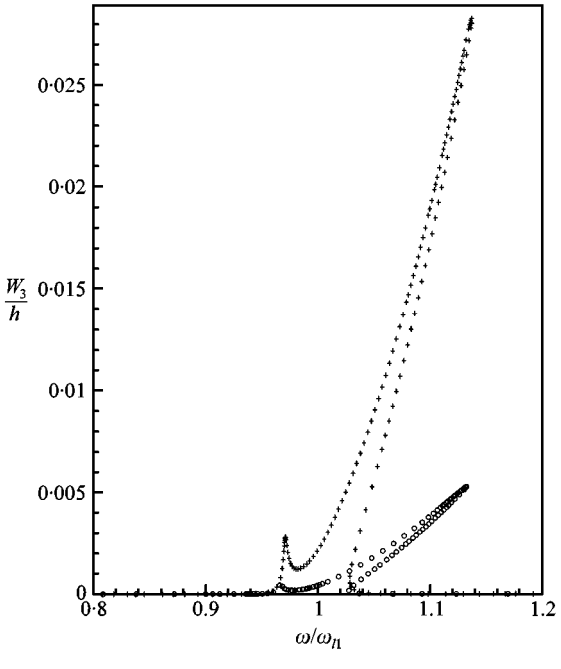

Figure 27. Third harmonic FRF at $(\xi, \eta) = (0{\cdot}5, 0{\cdot}5)$. Plate 2: ○ $\theta = 15°$; + $\theta = 45°$.

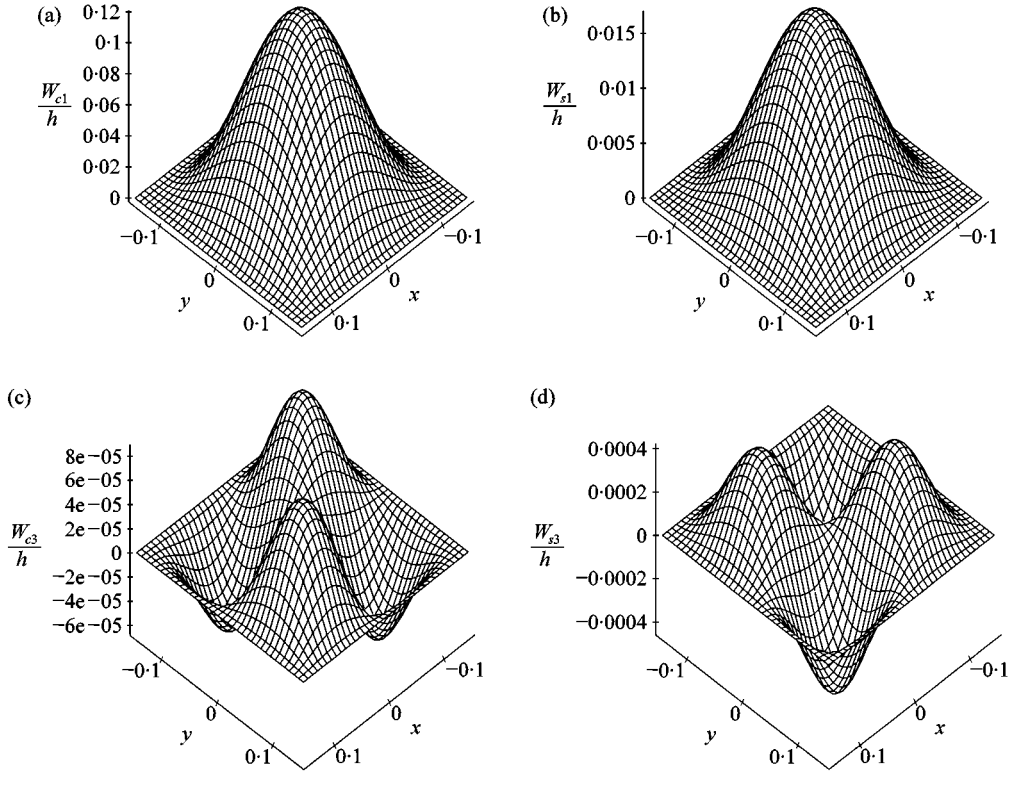

Figure 28. Deformation of Plate 2 ($\theta = 15^\circ$) at point $\omega/\omega_{l1} = 0{\cdot}9666$. (a) cos ($\omega t$); (b) sin ($\omega t$); (c) cos ($3\omega t$); (d) sin ($3\omega t$).

third harmonic is now associated with the sixth and the seventh modes and is very lightly excited.

4. CONCLUSIONS

In this paper, the steady state multi-harmonic response of isotropic and laminated plates was analyzed. Internal resonances of the type 1 : 3 were found. These occurred due to the excitation of modes with frequencies around three times the first resonance frequency and resulted in multi-modal, multi-frequency response. The stability of the solutions was analyzed, and it was shown that stable multi-modal solutions occur.

Super-harmonic resonances were detected, but, in the absence of internal resonances, their amplitudes of vibration displacement are small.

Due to modal coupling, high order modes are excited and more harmonics must be included in the solution. In fact, the reason why it is necessary to include the third harmonic in the analysis of Plates 1 and 2 [16], is the existence of internal resonance between the first and higher order modes.

By varying the fibre orientation within the layers of a laminated plate, the plate's characteristics are changed. Not surprisingly, this is a way of avoiding internal resonances between some modes and in a certain frequency region.

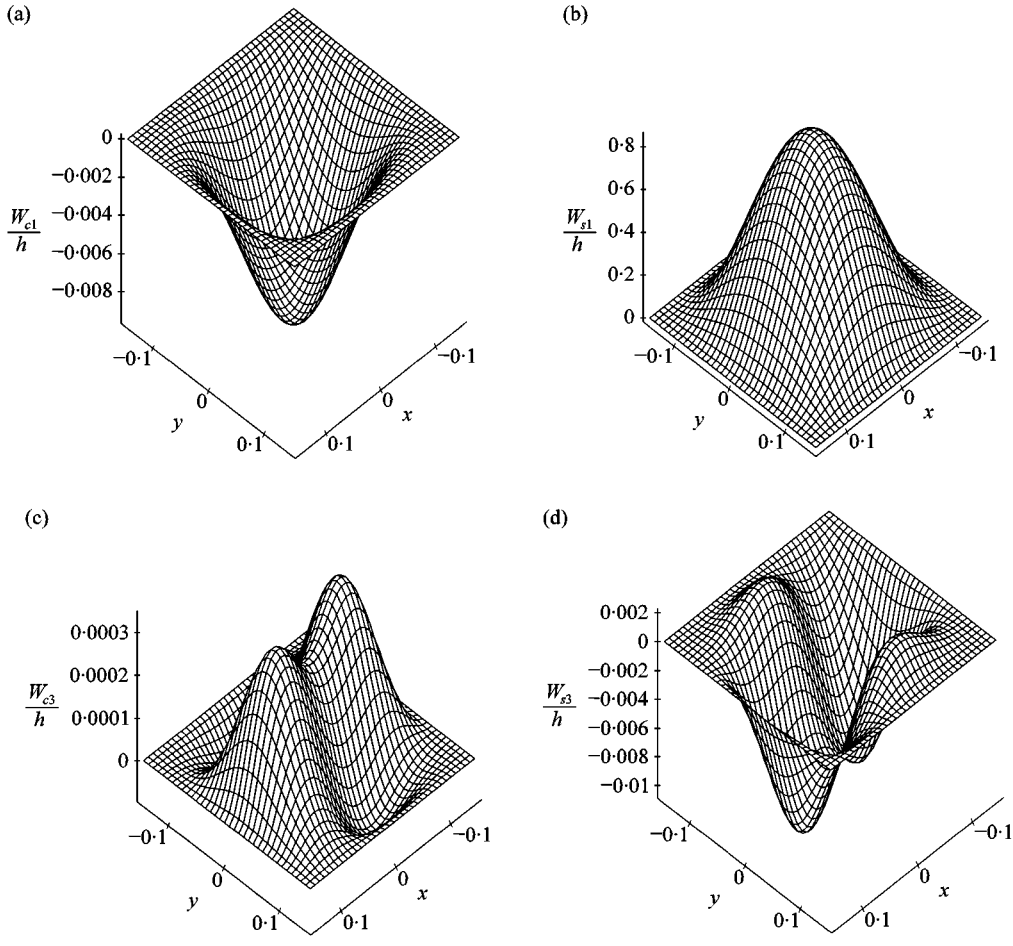

Figure 29. Deformation of Plate 2 ($\theta = 15^\circ$) at point $\omega/\omega_{l1} = 1{\cdot}1331$. (a) cos ($\omega t$); (b) sin ($\omega t$); (c) cos ($3\omega t$); (d) sin ($3\omega t$).

The fibre orientation also affects the hardening spring effect of the plate. For the same amplitude and non-dimensional frequency of excitation, Plate 2 attained lower vibration amplitudes if $\theta = 15^\circ$ than if $\theta = 45^\circ$.

ACKNOWLEDGMENT

P. Ribeiro gratefully acknowledges the scholarship PRAXIS XXI/BD/3868/94 from the *Fundação para a Ciência e a Tecnologia*, Portugal.

REFERENCES

1. R. M. Rosenberg 1966 *Advances in Applied Mechanics* **9**, 155–242. On non-linear vibrations of systems with many degrees of freedom.

2. R. BENAMAR, M.M. BENNOUNA, R. G. WHITE 1994 *Journal of Sound and Vibration* **175**, 377–395. The effects of large vibration amplitudes on the mode shape and natural frequencies of thin elastic structures. Part III: Fully clamped rectangular isotropic plates-measurements of the mode shape amplitude dependence and the spatial distribution of harmonic distortion.
3. H. WOLFE 1995 *Ph.D. Thesis, University of Southampton.* An experimental investigation of non-linear behaviour of beams and plates excited to high levels of dynamic response.
4. W. HAN 1993 *Ph.D. Thesis, University of Southampton.* The analysis of isotropic and laminated rectangular plates including geometrical non-linearity using the p-version finite element method.
5. W. HAN and M. PETYT 1997 *Computers and Structures* **63**, 295–308. Geometrically non-linear vibration analysis of thin, rectangular plates using the hierarchical finite element method—I: The fundamental mode of isotropic plates.
6. W. HAN and M. PETYT 1997 *Computers and Structures* **63**, 309–318. Geometrically non-linear vibration analysis of thin, rectangular plates using the hierarchical finite element method—II: 1st mode of laminated plates and higher modes of isotropic and laminated plates.
7. W. SZEMPLINSKA-STUPNICKA 1990 *The Behaviour of Non-linear Vibrating Systems.* Dordrecht: Kluwer Academic Publishers.
8. A. H. NAYFEH and D. T. MOOK 1995 *Nonlinear Oscillations.* New York: Wiley.
9. A. H. NAYFEH and B. BALACHANDRAN 1989 *Applied Mechanics Review* **42**(11—Part2), S175–S201. Modal interactions in dynamical and structural systems.
10. K. OH and A. H. NAYFEH 1998 *Journal of Vibration and Acoustics* **120**, 579–587. High- to low-frequency modal interactions in a cantilever composite plate.
11. S. L. LAU, Y. K. CHEUNG and S. Y. WU 1984 *Transactions of the ASME, Journal Applied Mechanics* **51**, 837–845. Non-linear vibration of thin elastic plates. Part 1: Generalized incremental Hamilton's principle and element formulation.
12. S. L. LAU, Y. K. CHEUNG and S. Y. WU 1984 *Transactions of the ASME, Journal Applied Mechanics* **51**, 845–851. Non-linear vibration of thin elastic plates. Part 2: Internal resonance by amplitude-incremental finite element.
13. B. ABE, Y. KOBAYASHI and G. YAMADA 1998 *International Journal of Non-Linear Mechanics* **33**, 675–690. Two-mode response of simply supported, rectangular laminated plates.
14. P. RIBEIRO and M. PETYT *International Journal of Non-linear Mechanics* Non-linear free vibration of isotropic plates with internal resonance (accepted).
15. P. RIBEIRO and M. PETYT *Journal of Sound and Vibration* **225**, 127–152. Multi-modal geometrical nonlinear free vibration of composite laminated plates.
16. P. RIBEIRO and M. PETYT *Journal of Sound and Vibration* **226**, 955–983. Geometrical non-linear, steady state, forced, periodic vibration of plates. Part I: Model and convergence studies.
17. C. HAYASHI 1964 *Nonlinear Oscillations in Physical Systems.* New York: McGraw-Hill.
18. P. RIBEIRO 1998 *Ph.D. Thesis, University of Southampton.* Geometrical non-linear vibration of beams and plates by the hierarchical finite element method.
19. P. RIBEIRO and M. PETYT *International Journal of Mechanical Sciences Science* **41**, 437–459. Non-linear vibration of plates by the hierarchical finite element and continuation methods.
20. R. LEWANDOWSKI 1997 *International Journal Solids and Structures* **34**, 1925–1947. Computational formulation for periodic vibration of geometrically nonlinear structures—Part 1: Theoretical background.
21. R. SEYDEL 1988 *From Equilibrium to Chaos. Pratical Bifurcation and Stability Analysis.* New York: Elsevier.